CrystEngComm

ROYAL SOCIETY OF CHEMISTRY

PAPER

View Article Online
View Journal | View Issue

Cite this: *CrystEngComm*, 2025, **27**, 921

Competition between sigma and Pi holes on the same atom

Steve Scheiner

Received 27th November 2024,
Accepted 21st January 2025

DOI: 10.1039/d4ce01194e

rsc.li/crystengcomm

Quantum chemical calculations compare the ability of σ and π-holes on the same atom to engage in a noncovalent bond. The first series of Lewis acids are the hypervalent XR_3 series where X refers to a central halogen atom. These molecules adopt a T-shape with a π-hole above the molecular plane and a σ-hole along the extension of the vertical of the T. A similar T-shape is characteristic of the AeX_2Y series where Ae is an aerogen/noble gas atom and Y is a chalcogen O or S. In all of these cases the σ-hole is deeper and forms a stronger bond with a NH_3 base. Also studied is a set of MX_2 and MX_3 units where M refers to a transition metal atom. Despite a variety of molecular shapes, encompassing planar trigonal, T-shape, bent, and linear, there is only one sort of hole present on each M atom, either σ or π. Other sorts of molecules also contain only a π-hole although the shape allows the possibility in principle of a σ-hole as well.

Introduction

Following many years of intense study of the many facets and applications of the H-bond,[1–9] it was realized that there are a host of closely related noncovalent bonds. In each of these interactions, the bridging proton of the H-bond is replaced by another element, typically but not always from the right side of the periodic table. These so-called triel, tetrel, pnicogen, chalcogen, and halogen bonds are eponymous labels arising from the particular family of elements from which this bridging atom is drawn. These atoms do not necessarily bear an overall positive atomic charge, but nonetheless are characterized by a small region of positive charge which typically lies directly along the extension of the R–X covalent bond, where X refers to the bridging atom and R to the atom to which it is covalently attached. The positive potential is due in large part to the displacement of electron density that occurs when a σ(RX) bonding orbital is formed and occupied, shifting density to the internuclear region from the outside, peripheral areas. This motion leaves a deficiency of density in what has come to be known as a σ-hole, along the extension of the R–X axis.[10–21] It is for this reason that this entire set of noncovalent bonds fall into a general category of "σ-hole bond". Of course, like the parent H-bond, these interactions do not rely entirely on the coulombic attraction of a positive σ-hole with the negative region of a partner nucleophile, but are supplemented by forces such as charge transfer, polarization, and dispersion. Even though these σ-hole bonds are based on a small positive σ-hole, rather than a positively charged H atom in its entirety, their strength can match and exceed what is found in the H-bond. For example, a P···N pnicogen bond between O_2NPH_2 and NH_3 reaches an interaction energy above 8 kcal mol^{-1}.[22] As a more extreme example, a Sn···N tetrel bond between F_3ClSn and NH_3 climbs up to 38 kcal mol^{-1}.[23]

As work on σ-hole bonds progressed, it was soon realized that the idea is not limited simply to the region along the extension of the R–X covalent bond. The planar H_2CO formaldehyde molecule furnishes a classic example. The electronegative O atom might certainly draw density toward itself and propagate the beginnings of a σ-hole along the C═O axis near the C atom. But any such σ-hole would be dwarfed by the more proximate positive H atoms which would draw a nucleophile toward themselves to generate a CH···Nuc H-bond. On the other hand, if one looks above the molecular plane, the formation of the π-bonding orbital draws density toward the region between the C and O atoms, depleting the density that lies outside these two atoms. Since C is much less electronegative than is O, the π-orbital is polarized toward the O, further amplifying the depletion of density above the C atom. The positive area above the C atom and the molecular plane is termed a π-hole.[24,25] The interaction of a nucleophile with the C atom falls under the heading of a tetrel bond, but this idea extends over the full range of noncovalent bond types. For example, a nucleophile can interact with the π-hole above the Se atom of planar SeO_3 in what would be analogously termed a chalcogen bond, and so on for a wide range of planar molecules.

The array of different systems that present π-holes is impressively diverse.[25,26] As alluded to above, despite its fairly high electronegativity, the C atom acquires a π-hole within the context of a carbonyl group as in formaldehyde

Department of Chemistry and Biochemistry, Utah State University, Logan, Utah 84322-0300, USA. E-mail: steve.scheiner@usu.edu

and related systems,[27–31] a hole which is accentuated for larger tetrel atoms such as Ge.[25,32] Planar TrR_3 units are prominent amongst these, where the π-hole lies directly above the central triel Tr atom.[33–36] A similarly shaped molecule, but with a chalcogen at its center, SeO_3 contains a π-hole above the Se.[25] Another hypervalent atom, this time a halogen as in $NBrO_2$, places the Br at the center of a planar triangle, with a π-hole centered above it.[25] Another triangular shaped molecule which also induces a π-hole of sorts is T_3H_6, where T refers to C or any other tetrel atom.[37] The overall structure can be extended to square planar as in ZnF_4, which places a π-hole directly above the central metal atom;[38] likewise for XeF_4 (ref. 25) or related systems[39] with an aerogen/noble gas at its center. A square pyramidal geometry can place a π-hole on a metal atom like Mo opposite the O atom at the pyramid apex in what is termed a wolfium bond.[40] The presence of the electron-withdrawing O atoms provides the N atom of the planar NO_2 group with a robust π-hole, allowing its N to serve as electron acceptor.[25,27,41,42] Replacement of the central N by the heavier pnicogen As in $FAsO_2$ (ref. 25) or other related systems containing P[27,43] leaves the π-hole intact. Even the normally unreactive noble gas/aerogen atoms can acquire a π-hole, as for example in planar $XeOF_2$.[44]

While the electrostatic potential lying above the center of the benzene ring is negative, adding a number of electron-withdrawing substituents such as halogen can suck out sufficient electron density to reverse the sign of the potential, resulting in a π-hole above the ring,[31,45] rather than being attached to any one particular atom. Other six-membered rings with π-holes above them include heterocyclic systems such as 1,3,5-triazine.[46] Linear molecules can also harbor a π-hole,[47] typically in the form of a ring of positive potential that encircles the molecule as for example alkynes,[31] the nitrile group,[48,49] CO_2,[32] or more exotic systems such as NSeN, FCaF, and FGaO (ref. 47) or $Zn(CCH)_2$.[50] It should be stressed that π-holes are more than just a theoretical construct, having been observed directly by Kelvin probe force microscopy[51] of 9,10-dichlorooctafluoroanthracene.

Given the occurrence of positively charged regions of both σ and π types, it is natural to wonder about their relative ability to interact with an approaching nucleophile, how they might compete with one another. In other words, are σ-hole bonds intrinsically stronger than their π-hole counterparts, or *vice versa*? While quite a few molecules contain both sorts of holes, they are typically present on different atoms,[52,53] making a direct comparison a difficult apples-and-oranges question. There are a few papers in the recent literature that have addressed this question by identification and study of molecules containing both σ and π-holes on the same atom. Varadwaj *et al.*[54] have recently pointed out that the T-shaped CF_3IX_2 molecules contain both sorts of hole on the central I atom. Within the context of a crystal, these molecules engage in a variety of interactions with one another which allowed both of these sorts of holes to serve as electron donors, along with several other noncovalent bond types. These bond types survived removal of dimers from the crystal and full geometry optimizations by quantum chemical calculations, so can be considered reasonably robust. Nonetheless, the examination was unable to answer the basic question as to which type of hole is preferred. These results amplified earlier quantum calculations of the IF_3 Lewis acid and its complex with a base[25] as well as the closely related BrF_3.[26] Another sort of system which places both a σ and π-hole on the same atom is the $AeOF_2$ series which was studied recently for the cases of Ae = Kr and Xe (ref. 44) and their association with assorted diazines. Comparisons of the binding were however somewhat clouded by the formation of secondary H-bonding interactions.

The present work is designed to answer the specific question as to whether it is the σ or π-hole to which a nucleophile is preferentially attracted when both sites occur on the same atom. The first class of molecules where such a confluence of sites occurs is XR_3, where X is a halogen atom and R represents any of a number of different groups. The hypervalent bonding of the central X leads to a T-shaped molecule, with a σ-hole on the X, opposite the R at the base of the stem, and a π-hole above the molecular plane. Another sort of molecule that also adopts a T-shape is the $AeYX_2$ unit, wherein Ae, Y, and X refer respectively to an aerogen, chalcogen, and halogen atom. A σ-hole is present opposite the Y, supplemented by π-holes above and below the Ae. The position and depth of each such hole on the molecule is first assessed *via* DFT calculations for purposes of comparison. A nucleophile is then positioned near each hole and allowed to form a dyad *via* a halogen or aerogen bond, respectively. The strengths and other properties of these σ and π-hole bonds are then compared, and related back to the depths of the two holes.

Methods

Full optimizations of isolated monomers and dimers were performed at the M06-2X/def2TZVP level of theory[55–57] using the Gaussian 16 (Rev. C.01) package.[58] M06-2X has been repeatedly assessed to be one of the most accurate functionals for noncovalent interactions.[59–67] Harmonic frequency analysis confirmed their nature as true minima. The Boys–Bernardi counterpoise approach[68] corrected the basis set superposition error (BSSE). The MEP (molecular electrostatic potential) was analyzed to identify the maxima on the 0.001 au isodensity surface of the isolated monomers, utilizing the MultiWFN software,[69,70] which was also applied to generate electron localization functions (ELFs). The AIMAll program[71] provided QTAIM topological analysis[72,73] of the electron density as represented by bond paths and their bond critical points.

Results

Halogen bonds

Fig. 1a illustrates the MEP surrounding the $IBrF_2$ molecule as an example of the entire set of IX_3 molecules. There is an intense blue region to the right of I which represents the

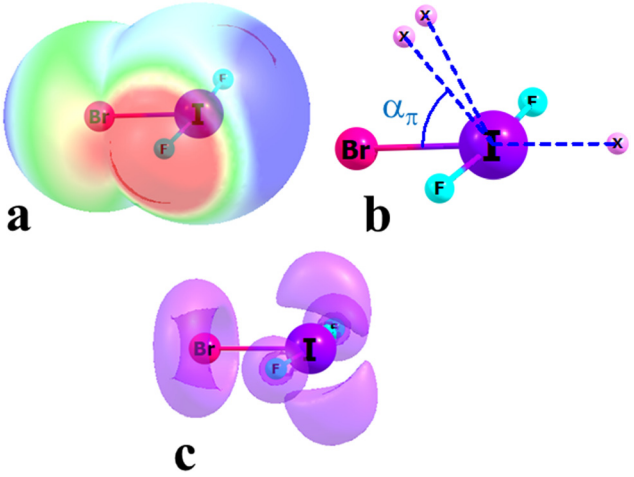

Fig. 1 a) MEP surrounding IF_2Br where blue and red regions refer respectively to positive and negative potential. b) Locations of maxima of the MEP on the 0.001 au isodensity surface marked by X, c) ELF diagram showing bond and lone electron pairs.

positive potential along the Br–I σ-hole. The precise point where this MEP has its maximum on the 0.001 au isodensity surface is indicated by the X site in Fig. 1b. There are also maxima above the plane of the molecule which are visible as the light blue area in Fig. 1a. This region is characterized by two maxima, fairly close together, as shown by the other X sites in Fig. 1b. The angle these π-sites make with the I–Br axis are designated as α_π. The IF_2Br row of Table 1 shows that the value of the MEP at these σ and π maxima are 45.1 and 16.5 kcal mol^{-1}, respectively, with the σ-hole deeper by 28.6 kcal mol^{-1}.

It is obvious that the π maxima are somewhat removed from a position directly above the I atom, with α_π angles of only 65°, considerably less than 90°. The principal reason for this displacement arises in connection with the two lone pairs on the central I atom. As is evident in the ELF diagram of Fig. 1c, the density associated with these lone pairs pushes the electron-deficient π-hole toward the Br. The splitting of each π-hole into two separate maxima can be traced to the primary positions of the I lone pairs in the plane perpendicular to the molecule and intersecting the Br–I axis. The gap between these lone pairs facilitates the presence of the σ-hole directly along the Br–I bond extension. This gap also helps explain why the σ V_{max} is larger than the π quantity.

When NH_3 is brought in to form a complex with BrF_2I it can engage with either the σ or π-hole, to form the structures in Fig. 2a and b, respectively. Although the σ-hole lies directly along the Br–I axis, there is a slight nonlinearity in the σ complex, where θ_σ is 160.6°, as listed in Table 2. When approaching the π-hole, the N conforms to the V_{max} location, as θ_π = 72.0°, only 7° from the π maximum of α_π = 65.4°. Also connecting with the MEP maxima on either side of the bisecting plane in Fig. 1b, the NH_3 is displaced closer to one F than to the other. Given the much deeper σ-hole as compared to π, it is not surprising that the σ interaction energy of 12.35 kcal mol^{-1} substantially exceeds the corresponding π energy of 4.67 kcal mol^{-1}, as reported in Table 1.

The upper half of Table 1 documents the hole depths and energetics of the full range of IX_3 molecules. Many of the trends contained therein are consistent with chemical intuition. As the F atoms of IF_3 are replaced with the less electronegative Cl and then Br, both of the holes over the I atom become shallower. In the $IF_3 > ICl_3 > IBr_3$ series, for example, the σ V_{max} drops from 57.5 kcal mol^{-1} down to 49.4 and then 46.3. The π-hole also becomes shallower, albeit less sharply, with V_{max} diminishing by only 3.6 kcal mol^{-1}. The reduction in the π-hole depth is a bit sharper when only one of the three F atoms is replaced by Cl or Br. It may be noted finally that introduction of an electron-releasing methyl group dramatically reduces the two hole depths, to the point where the maximum in the π region disappears entirely.

The third column of Table 1 shows that the σ-hole remains substantially deeper than its π cousin. It is thus

Table 1 Hole depths of monomers and interaction energies and BCP densities of complexes with NH_3

	V_{max}, kcal mol^{-1}			$-E_{int}$, kcal mol^{-1}			ρ_{BCP}, 10^{-4} au		
	σ	π	σ–π[a]	σ	π	σ–π[a]	σ	π	σ–π[a]
IF_3	57.5	22.7	34.8	14.68	5.75	8.93	355	152	203
IF_2Cl	49.4	18.2	31.2	13.16	4.83	8.33	351	115	236
IF_2Br	45.1	16.5	28.6	12.35	4.67	7.68	339	123	216
ICl_3	49.4	20.3	29.1	20.24	4.87	15.37	550	121	429
IBr_3	46.3	19.1	27.2	19.57	X	X	542	X	X
IBr_2Me	31.2	X	X	7.60	X	X	193	X	X
ClF_3	41.8	24.2	17.6	9.96	4.04	5.92	363	135	228
ClF_2I	17.6	15.9	1.7	5.37	4.39	0.98	217	90	127
ClF_2Me	12.6	X	X	3.70	X	X	126	X	X
ClF_2NH_2	21.6	3.6	18.0	5.21	X	X	176	X	X
$ClBr_2I$	23.8	19.2	4.6	9.67	5.12	4.55	346	112	234
$ClBr_3$	32.1	20.6	11.5	13.46	4.71	8.75	496	117	379
ClI_3	22.2	17.0	5.2	9.29	X	X	318	X	X

[a] Difference between σ and π values. X indicates absence of V_{max} or π-complex.

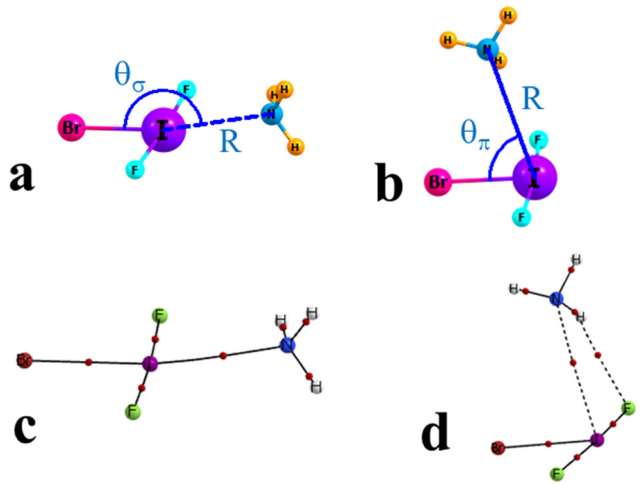

Fig. 2 a) σ and b) π geometries of complexes of NH_3 with IF_2Br, AIM diagrams of c) σ and d) π structures, where small red ball indicates location of bond critical point.

unsurprising that the interaction energies in the next columns of Table 2 reflect this by much stronger bonding for the σ complexes. The latter interaction energies range from 13 to 20 kcal mol^{-1}, while the π quantities are much smaller, all roughly 5 kcal mol^{-1}. In fact, despite the π V_{max} of 19.1 kcal mol^{-1} for IBr_3, its π-hole is not deep enough to sustain a π-complex with NH_3.

The lower section of Table 1 contains the corresponding data when the central I is replaced by Cl. The greater electronegativity of the latter, coupled with its lesser polarizability, leads to smaller values of V_{max}, particularly for the σ-holes. The π-holes, on the other hand, are more resilient to the I → Cl mutation. For example, V_{max} is equal to 19.1 kcal mol^{-1} for IBr_3 but is actually a little larger at 20.6 for $ClBr_3$. Nonetheless, σ-holes remain deeper than the π regions, even if by a smaller differential.

Consistent with the shallower Cl σ-holes, the interaction energies in Table 1 are smaller than those for I. The π interaction energies are barely affected by the change in central atom, remaining at roughly 5 kcal mol^{-1}. As a bottom line, the σ complexes are more strongly bound than their π correlates, even if by a smaller margin. The closest comparison arises in the context of ClF_2I where the two complex types are separated by only 0.98 kcal mol^{-1}.

More detailed perusal of Table 2 shows that the intermolecular separations of the σ complexes are shorter than those in the π structures, consistent with the stronger binding in the former. The difference in R is quite substantial, between 0.5 and 0.7 Å. Many of the θ_σ angles differ from the idealized 180°. Regarding the angular aspects of the π complexes, the NH_3 is not far removed from the 0.001 au maximum of the MEP, with θ_π not very different from α_π.

AIM analysis of the electron density topology helps to pinpoint specific bonding interactions. For example, the molecular diagram of the σ configuration of the $IF_2Br\cdots NH_3$ dyad in Fig. 2c shows a single bond path between the I and N atoms. As indicated by the relevant entry in Table 1, the density at the bond critical point is 0.0339 au. The corresponding density in the π-configuration is roughly 1/3 of this quantity, 0.0123 au, consonant with its smaller interaction energy. This observation of a larger BCP density for the σ XB in comparison to its π analogue is common to all of the systems in Table 1, where the ρ_σ/ρ_π ratio varies between 2.3 and 4.5.

One may note also in the diagram of the π-complex in Fig. 2d, that the I···N bond path is complemented by a second such path that is suggestive of a weak NH···F H-bond. Elucidation of the density at each bond critical point yields 0.0104 and 0.0123 au for the I···N and H···F contacts, respectively, suggesting that the latter cannot be ignored as a contributor to the total interaction energy. NBO analysis of this geometry adds to this finding. It shows 0.16 kcal mol^{-1} arising from charge transfer from the N lone pair to the IBr and IF antibonding orbitals, which compares with 0.57 kcal mol^{-1} associated with F lone pair transfer to the associated N–H antibonding orbitals. So the weaker binding in the π-complex occurs even in the presence of a secondary bonding force, bolstering the claim that the halogen bond itself is very much weaker than that in the σ geometry. (The

Table 2 Geometrical aspects (Å and degs) of complexes with NH_3 and positions of σ and π holes of monomers

	σ		π		
	R	θ_σ	R	θ_π	α_π
IF_3	2.695	158.6	3.173	61.6	60.1
IF_2Cl	2.712	161.0	3.340	70.4	64.0
IF_2Br	2.734	160.6	3.393	72.0	65.4
ICl_3	2.490	179.8	3.343	69.8	65.1
IBr_3	2.499	179.7	X	X	65.4
IBr_2Me	3.028	164.0	X	X	X
ClF_3	2.533	177.7	3.042	70.2	64.1
ClF_2I	2.779	165.5	3.227	75.9	63.3
$ClBr_2I$	2.564	179.6	3.135	77.2	64.0
ClF_2Me	3.022	156.2	X	X	X
ClF_2NH_2	2.859	163.4	X	X	75.6
$ClBr_3$	2.401	179.4	3.125	78.6	76.3
ClI_3	2.600	179.3	X	X	63.0

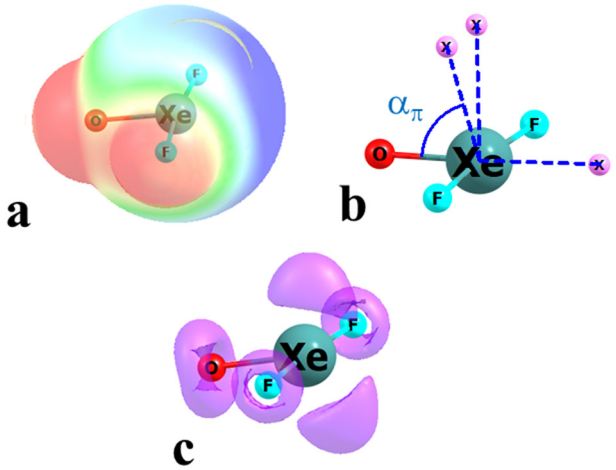

Fig. 3 a) MEP surrounding XeF_2O where blue and red regions refer respectively to positive and negative potential. b) Locations of maxima of the MEP on the 0.001 au isodensity surface, c) ELF diagram showing bond and lone electron pairs.

occurrence of the secondary bond path in the π-complex of Fig. 2d is not characteristic of all such geometries, but does occur in a number of them, *viz.* IF_2Cl, ICl_3, ClF_2I, $ClBr_2I$, and $ClBr_3$.) The weakness of the π XB, coupled with the electrostatic attraction between the positive H atoms of NH_3 and the negative substituents on the Lewis acid, is largely responsible for the skewing of the NH_3 and its N lone pair from a strict alignment with the central I/Cl atom's π-hole.

Aerogen bonds

Another class of molecules where the central atom can contain both σ and π-holes can be represented by $AeYX_2$, where Ae represents an aerogen/noble gas atom, Y a chalcogen like O or Se, and a halogen atom is indicated as X. One such example is $XeOF_2$, which is illustrated in Fig. 3a, along with its surrounding MEP. Like the XR_3 systems, these molecules also take on a planar T-shape. Their MEP contains a σ-hole directed along the Y-Ae axis. The first column of Table 3 shows that the σ-hole depths in this $AeYX_2$ class vary between 39 and 59 kcal mol^{-1}, comparable to the same quantities in the XR_3 class of Table 1. Also like the latter systems, Fig. 3b shows that $XeOF_2$ has a split π-hole with two closely spaced MEP maxima. The two Xe lone pairs apparent in Fig. 3c cause this splitting, as well as the α_π angles less than 90°. The σ-hole is quite a bit deeper than the π-hole, 59 *vs.* 34 kcal mol^{-1}. However, further inspection of Table 3 shows that the 0.001 au isodensity surface does not contain a π maximum for the other $AeYX_2$ monomers. This absence does not mean that the potential is not positive in this region, only that there is no strictly defined maximum on that particular isodensity surface. Taking the $XeOBr_2$ species as an example, although there is no π maximum on the MEP for ρ = 0.001 au, raising this density criterion to 0.002 au causes the appearance of such a maximum on this redefined surface, with V_{max} equal to +42.2 kcal mol^{-1}, as compared to V_{max} of 67.8 kcal mol^{-1} for the σ-hole on this same surface. Moreover, as explained below, the π-region is able to host the NH_3 nucleophile in a π-complex, notwithstanding the lack of such a MEP maximum for ρ = 0.001 au.

The geometries of the aerogen-bonded σ and π dyads of $XeOF_2$ with NH_3 are illustrated in Fig. 4a and b, respectively. The energetics in Table 3 yield interaction energies between 7 and 14 kcal mol^{-1} in the same general range as for the XR_3 complexes in Table 1. One difference between the two sorts of complexes is that the π aerogen bonds are stronger than are the π XBs, with interaction energies between 6 and 8 kcal mol^{-1}. Given the same substituents, the heavier Xe engages in stronger AeBs than does Kr. The σ geometries are more tightly bound by variable amounts, and in the cases where Y = Se, by less than 2 kcal mol^{-1}.

The AIM diagrams for these sorts of complexes are exemplified by those for $XeOF_2$ in Fig. 4c and d. The bond critical point densities of the AeB bond paths are listed in the last three columns of Table 3. Consistent with the stronger π AeBs as compared to their π XB analogues, so too are their values of ρ_{BCP}, which lie in the range between 0.014 and 0.017 au. The higher densities of the σ AeBs as compared to π is mirrored by their larger interaction energies.

The relevant geometrical parameters of the various complexes are displayed in Table 4. Consistent with their stronger bonding, the intermolecular distances are shorter for the σ as compared to π geometries. The mutation of the Y atom from O to Se leads to longer distances as well as lowered interaction energies. While the O–Ae···N alignments are very close to linear in the σ geometries, a nonlinearity of some 15° arises for the Se–Ae···N AeBs.

Transition metals

There are a set of other sorts of molecule where one might imagine either σ or π holes or both associated with a central

Table 3 Hole depths of monomers and interaction energies and BCP densities of complexes with NH_3

	V_{max}, kcal mol^{-1}			$-E_{int}$, kcal mol^{-1}			ρ_{BCP}, 10^{-4} au		
	σ	π	σ–π	σ	π	σ–π	σ	π	σ–π
XeF_2O	59.1	34.4	24.7	11.45	7.88	3.57	261	174	87
XeF_2Se	46.8	X	X	8.82	7.00	1.82	201	149	52
$XeBr_2O$	56.1	X	X	13.55	7.82	5.73	300	168	132
KrF_2O	57.0	X	X	10.80	7.00	3.80	267	170	97
KrF_2Se	39.3	X	X	7.21	6.50	0.71	180	144	36

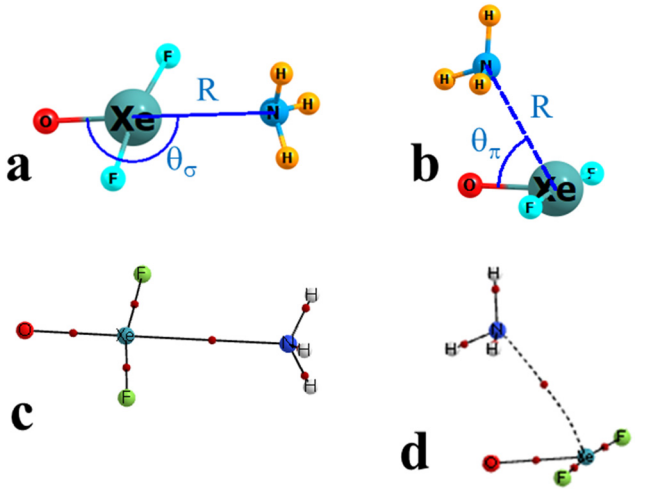

Fig. 4 a) σ and b) π geometries of complexes of NH_3 with XeF_2O, AIM diagrams of c) σ and d) π structures, where small red ball indicates location of bond critical point.

atom. The MCl_3 molecules where M refers to a transition metal occur either as D_{3h} planar molecules or as a T-structure.[38] Examples are provided in Fig. 5, and the associated quantitative aspects in Table 5. Both YCl_3 and $TcCl_3$ form equilateral triangles, and have a π-hole directly above the central metal, with no σ-hole. Despite the much deeper π-hole of the former, its M···N distance is much longer, and its interaction energy with NH_3 considerably smaller than $TcCl_3$. The ELF diagrams of both allow the growth of the π-hole, unimpeded by a lone pair on the central metal.

The situation is different for $NbCl_3$, as the Nb has associated with it a good deal of density which has the disposition of a d_{z^2} orbital. This density pushes V_{max} away from the perpendicular direction, making it intermediate between a π or σ hole, and reduces its magnitude to only 18.3 kcal mol^{-1}. As a result, the NH_3 occupies a position well off of the D_{3h} vertical axis, as evident in Fig. 5c, with a fairly small interaction energy of 27.8 kcal mol^{-1}. $AgCl_3$ presents a different scenario. The monomer takes on a T-shape, and contains only a σ-hole. Without any Ag lone pairs in its vicinity to dampen this hole, V_{max} is fairly large at 58.8 kcal mol^{-1}. The NH_3 nucleophile is coincident with the σ-hole in the monomer, yielding a sizable interaction energy of 40.0 kcal mol^{-1}.

MCl_2 molecules are also capable in principle of either a σ or π-hole as long as the molecule is not linear.[38] Fig. 6 illustrates several such units, along with their MEP, ELF, and

Table 4 Geometrical aspects (Å and degs) of complexes with NH_3 and positions of σ and π holes of monomers

	σ		π		
	R	θ_σ	R	θ_π	α_π
XeF_2O	2.882	179.5	3.072	71.3	86.0
XeF_2Se	3.015	163.2	3.175	78.5	X
$XeBr_2O$	2.808	179.5	3.105	70.3	X
KrF_2O	2.751	175.9	2.967	75.2	X
KrF_2Se	2.995	166.2	3.069	77.7	X

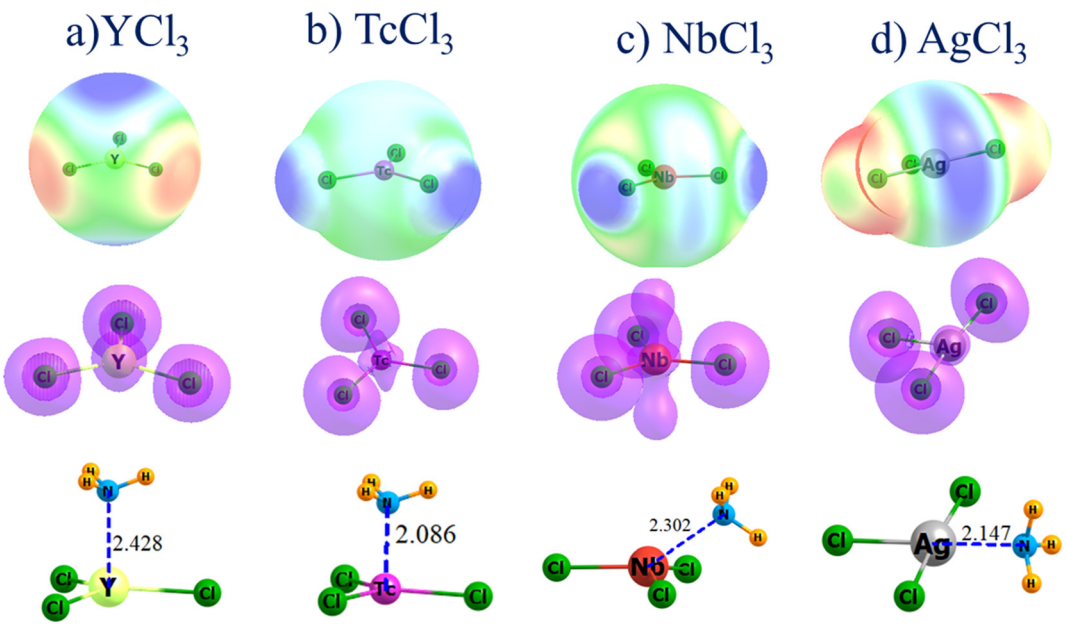

Fig. 5 MEP, ELF diagram, and geometry of complex with NH_3 of a) YCl_3, b) $TcCl_3$, c) $NbCl_3$, and d) $AgCl_3$. Distances in Å.

Table 5 Type and depth of σ/π hole in monomer, and intermolecular distance and interaction energy of complex with NH_3. Quantities in kcal mol^{-1}, and distance in Å

	Hole type	V_{max}	R	$-E_{int}$
YCl_3	π	161.0	2.428	38.60
$TcCl_3$	π	20.4	2.086	54.40
$NbCl_3$	σ/π	18.3	2.302	27.80
$AgCl_3$	σ	58.8	2.147	40.01
$MoCl_2$	σ	15.6	2.174	37.52
$RuCl_2$	σ	23.5	2.054	55.37
$PdCl_2$	σ	70.7	2.145	37.72
$CdCl_2$	π	51.4	2.412	22.76

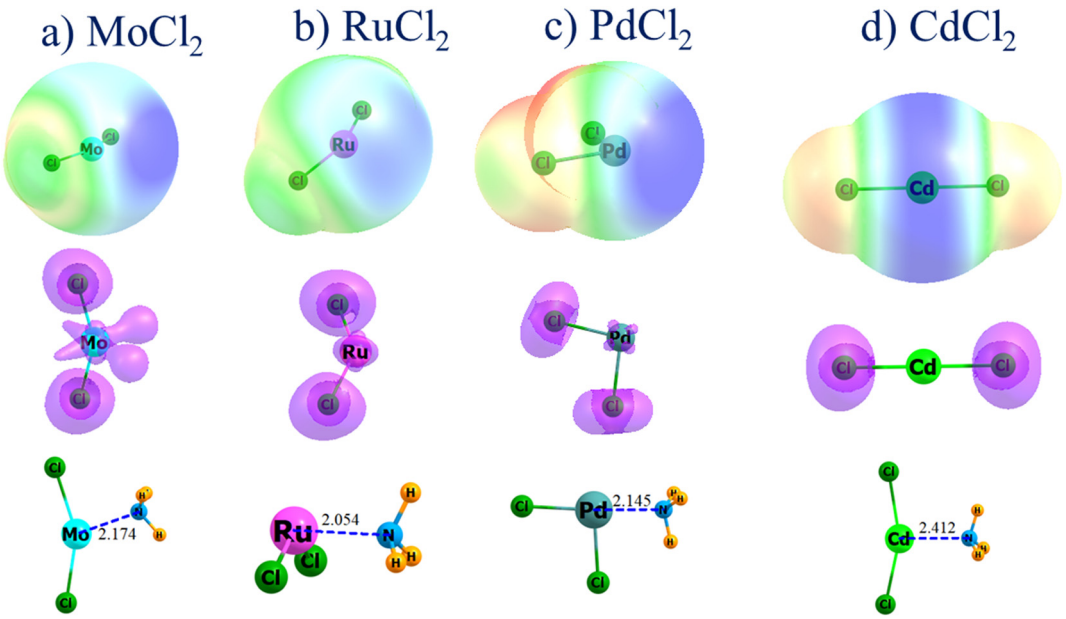

Fig. 6 MEP, ELF diagram, and geometry of complex with NH_3 of a) $MoCl_2$, b) $RuCl_2$, c) $PdCl_2$, and d) $CdCl_2$. Distances in Å.

complex with NH_3. The MEP maxima of bent $MoCl_2$ lie in the molecular plane as σ-holes. Their positions are adjusted and their potential modulated by the density of the Mo lone pairs in Fig. 6a, so V_{max} is only 15.6 kcal mol^{-1}. $RuCl_2$ has no such lone pairs so the MEP maxima are somewhat larger. The absence of these lone pairs allows the NH_3 to take up a position as illustrated in Fig. 6b, even in the absence of a formal MEP maximum at this location. $PdCl_2$ in Fig. 6c places the NH_3 much closer to its σ-hole positions, guided there by the very deep hole, with V_{max} equal to 70.7 kcal mol^{-1}. Since $CdCl_2$ is linear, it is encircled by a belt of positive potential, an extended π-hole of a sort. It is this belt to which the NH_3 is attracted in Fig. 6d. Although V_{max} is rather large for this subunit at 51.4 kcal mol^{-1}, the interaction energy is fairly small, only 22.76 kcal mol^{-1}.

So in summary, the MCl_n systems contain either a σ or π-hole on the central metal atom but not both. There is no set rule which makes dimers with either sort of hole more strongly bound than the other. But it should be emphasized that the large interaction energies, and other facets of many of these transition metal complexes,[38] lead to their characterization as containing a large component of covalency.

Other systems

Other types of systems were examined in an attempt to identify those which might contain both a σ and π-hole on the same atom. The planar R_2CO class of carbonyls is known to contain a π-hole above the carbonyl group capable of sustaining a tetrel bond with a nucleophile. However, H_2CO does not generate a σ-hole in the molecular plane. It was thought that perhaps a σ-hole might be generated by replacing C by its larger tetrel congener Ge. This replacement did intensify the π-hole, yielding V_{max} values of 57.1 and 82.5 kcal mol^{-1}, respectively, in H_2GeO and F_2GeO. However, in neither case did a σ-hole appear in the molecular plane. Nor was there a corresponding minimum found when NH_3 was placed opposite the O═Ge axis.

The planar TrX_3 species wherein Tr refers to a triel atom in the B family, is well known to engage in a triel bond through the π-hole above the Tr. Even with a heavier Tr atom

like Ga, it was not possible to form a σ-hole in the molecular plane to complement the π-hole. The V_{max} for GaF_3 and $GaBr_3$ were calculated to be 99.3 and 56.6 kcal mol^{-1}, respectively, which led to complexes with NH_3 having corresponding interaction energies of 48.43 and 39.05 kcal mol^{-1}. However, there is no σ-hole, nor can either molecule interact favorably with NH_3 in its molecular plane.

A final attempt was made with SeO_3, also trigonal planar, but with three Se═O double bonds. This molecule contained a π-hole with V_{max} equal to 62.0 kcal mol^{-1}, but with no MEP maximum in its plane. The π-hole sustained a chalcogen bond with NH_3 with an interaction energy of 33.18 kcal mol^{-1}, but no minimum could be located with the nucleophile in the SeO_3 plane.

Discussion

There are a number of points of comparison of some of the data presented here and prior reports. The bond critical point densities computed by Varadwaj *et al.*[54] for homodimers of CF_3IX_2 were in the general range of 0.0100–0.0200 au, comparable to the same quantities for the I···N π halogen bonds calculated here, albeit less than what was found for the σ XBs. The interaction energies for these dimers comprised an aggregate set of bonds but utilized halogen atoms rather than the stronger N nucleophile of NH_3, so were generally smaller than those reported in Table 1.

The displacement of a π-hole away from its purely perpendicular direction by a nearby lone pair was noted earlier in the context of XeF_4 where the Xe lone pairs cause a nucleophile to approach the central Xe from *a* direction off of the vertical.[25] Although the interaction energies of the aerogen bonds were complicated by secondary interactions,[44] the binding of an assortment of diazines to $AeOF_2$ echoed the stronger interactions with the Ae σ-hole for Kr and Xe. The preference for the σ-hole of $XeOF_2$ was reinforced by earlier computations with N-bases and anions.[74] The computed interaction energy with NH_3 in the σ-structure was quite close to the value exhibited here in Table 5. $XeOF_2$ was also studied when complexed to MeCN.[75] Unfortunately, analysis of the π-structure was complicated by the appearance of a subsidiary C···O tetrel bond. Even with that advantage, the π-geometry was less stable than the σ structure. The TX_2 dihalometallylene family where T represents a tetrel atom presents the possibility of σ-holes opposite each T–X bond and π-holes above and below the molecular plane, where the two σ-holes flank the T lone pair. Calculations[76] show that the π-holes are deeper than the σ-holes on the T atom.

The original concept of a π-hole rests on the idea of a strictly planar or linear geometry. But there are geometries where the distinction between a σ and π-hole may become a bit murkier. For example, there have been attempts to expand the π-hole idea to encompass a nonplanar, trigonal pyramid monomer such as those containing trivalent pnicogen atoms.[77] This geometry would of course preclude a π-hole as such. However, the approach of a nucleophile can cause an internal rearrangement, which pushes the geometry toward a trigonal bipyramidal framework. This sort of formal penta-coordination encompasses four ligands in total, plus a lone pair on the central atom. There are several ways in which the equatorial and axial sites can be occupied by the original ligands. If the three original ligands are located in the three equatorial positions, the pseudoplanar geometry contains a π-hole opposite the lone pair, to which the nucleophile can attach. On the other hand, their occupation of two equatorial and one axial site leads to only σ-holes each opposite a different ligand. Yet another situation places the ligands on one equatorial and two axial sites, which results in only a single σ-hole. These cases require very different magnitudes of deformation energy to transition from the original trigonal pyramid, so the interaction energy can differ substantially from the reaction or binding energy, somewhat clouding the question as to which hole is preferred.

Another example arises in the context of a hypervalent YX_4 molecule such as SeF_4. The geometry of this molecule is see-saw, with a pair of σ-holes opposite to the Se–F bonds serving as the legs of this see-saw.[77,78] Each of these two σ-holes can attract a nucleophile like NH_3. But another possible geometry occurs when the SeF_4 is deformed into a square by the approaching base. This planar structure now contains a pair of π-holes above and below the Se center. In sum, while the isolated monomer is nonplanar and contains no π-holes, geometric distortion caused by a nucleophile can in turn clear the way for the appearance of such a hole.

Even when the geometry of the monomer itself is planar, the distinction between a σ and π-hole is not always obvious. $NbCl_3$ provides one such example. Although this molecule adopts a planar trigonal shape, the electron density situated above the Nb center shown in Fig. 5c repels what would be a π-hole closer to the molecular plane. The nucleophile thus locates itself in a position intermediate between σ and π, roughly 50° from the vertical pseudo-C_3 axis of the $NbCl_3$.

Conclusions

The presence of both a σ and π-hole on the same atom is unusual, but does occur on occasion. The XR_3 species are a case in point, where X refers to a central halogen atom. The presence of two lone pairs on the central X causes these molecules to take on a planar T-shape. The π-hole above the plane is complemented by a σ-hole opposite the atom located at the vertical leg of the T. The σ-hole is deeper than the π-hole, as the latter is weakened and shifted by the proximity of the two lone pairs on the central X atom. The σ-hole sustains a stronger corresponding halogen bond with a nucleophile, by between 20% and 70%.

The $AeYX_2$ class of molecules, where Ae refers to an aerogen/noble gas atom, adopts a similar T-shape with the Y═O or S at the base of the T. As in the XR_3 cases, the two Ae lone pairs weaken the π-hole to the point that it disappears as a formal maximum on the 0.001 au isodensity surface. Nonetheless, the positive MEP in this π-region is

sufficient to sustain an AeB with a nucleophile, albeit one with a weaker bond than when the base approaches the σ-hole.

A transition metal M as the central atom offers a diverse set of MX_n molecules. Those systems where X = Cl and n = 2 or 3 present planar systems which could in principle host both σ and π-holes on M. Nonetheless, although some systems contain a σ-hole and others present a π-hole, there are none which contain both of them. The geometries of their complexes with a nucleophile are thus of only a single type, corresponding to the class of hole present on the Lewis acid. Other planar molecules were examined for the possible presence of both σ and π-holes. The tetrel H_2TO class, the triel GaX_3, and the chalcogen SeO_3 are all planar trigonal, and contain only a π-hole, which is reflected in the appearance of only one type of geometry when bonded to a nucleophile.

It is concluded that in those cases where both sorts of positive regions are present, it is the σ-hole which is deeper than the π-hole, and which sustains the stronger noncovalent bond with a nucleophile.

Data availability

The data discussed here are available from the author upon request.

Conflicts of interest

There are no conflicts to declare.

Acknowledgements

This material is based upon work supported by the U.S. National Science Foundation under Grant No. 1954310.

References

1 G. C. Pimentel and A. L. McClellan, *The Hydrogen Bond*, Freeman, San Francisco, 1960.
2 S. N. Vinogradov and R. H. Linnell, *Hydrogen Bonding*, Van Nostrand-Reinhold, New York, 1971.
3 S. Scheiner and L. Wang, *J. Am. Chem. Soc.*, 1993, **115**, 1958–1963.
4 G. A. Jeffrey and W. Saenger, *Hydrogen Bonding in Biological Structures*, Springer-Verlag, Berlin, 1991.
5 M. M. Szczesniak, S. Scheiner and Y. Bouteiller, *J. Chem. Phys.*, 1984, **81**, 5024–5030.
6 G. Orlova and S. Scheiner, *J. Phys. Chem. A*, 1998, **102**, 4813–4818.
7 M. Cuma, S. Scheiner and T. Kar, *J. Mol. Struct.: THEOCHEM*, 1999, **467**, 37–49.
8 S. Scheiner, *Hydrogen Bonding: A Theoretical Perspective*, Oxford University Press, New York, 1997.
9 G. Gilli and P. Gilli, *The Nature of the Hydrogen Bond*, Oxford University Press, Oxford, UK, 2009.
10 T. Clark, M. Hennemann, J. S. Murray and P. Politzer, *J. Mol. Model.*, 2007, **13**, 291–296.
11 P. Politzer and J. S. Murray, in *Noncovalent Forces*, ed. S. Scheiner, Springer, Dordrecht, Netherlands, 2015, pp. 357–389.
12 J. E. Del Bene, I. Alkorta and J. Elguero, *J. Phys. Chem. A*, 2013, **117**, 11592–11604.
13 S. J. Grabowski, *Phys. Chem. Chem. Phys.*, 2014, **16**, 1824–1834.
14 S. J. Grabowski, *Chem. – Eur. J.*, 2013, **19**, 14600–14611.
15 D. Quinonero, *Phys. Chem. Chem. Phys.*, 2017, **19**, 15530–15540.
16 S. A. C. McDowell, *Chem. Phys. Lett.*, 2014, **598**, 1–4.
17 S. Scheiner, *Phys. Chem. Chem. Phys.*, 2021, **23**, 5702–5717.
18 A. Bauzá and A. Frontera, *Coord. Chem. Rev.*, 2020, **404**, 213112.
19 I. Alkorta, J. Elguero and A. Frontera, *Crystals*, 2020, **10**, 180.
20 F. Nunzi, D. Cesario, F. Tarantelli and L. Belpassi, *Chem. Phys. Lett.*, 2021, **771**, 138522.
21 V. d. P. N. Nziko and S. Scheiner, *J. Phys. Chem. A*, 2014, **118**, 10849–10856.
22 S. Scheiner, *J. Phys. Chem. A*, 2011, **115**, 11202–11209.
23 S. Scheiner, *J. Phys. Chem. A*, 2021, **125**, 308–316.
24 S. Scheiner, *J. Comput. Chem.*, 2022, **43**, 1814–1824.
25 S. Scheiner, *J. Phys. Chem. A*, 2021, **125**, 6514–6528.
26 S. J. Grabowski, *Phys. Chem. Chem. Phys.*, 2017, **19**, 29742–29759.
27 J. S. Murray, P. Lane, T. Clark, K. E. Riley and P. Politzer, *J. Mol. Model.*, 2012, **18**, 541–548.
28 Y. Wei and Q. Li, *Mol. Phys.*, 2018, **116**, 222–230.
29 W. Dong, B. Niu, S. Liu, J. Cheng, S. Liu and Q. Li, *ChemPhysChem*, 2019, **20**, 627–635.
30 V. Angarov and S. Kozuch, *New J. Chem.*, 2018, **42**, 1413–1422.
31 P. R. Varadwaj, A. Varadwaj, H. M. Marques and K. Yamashita, *CrystEngComm*, 2023, **25**, 1411–1423.
32 M. Hou, Z. Liu and Q. Li, *Int. J. Quantum Chem.*, 2020, **120**, e26251.
33 J. Echeverría, *CrystEngComm*, 2017, **19**, 6289–6296.
34 P. Politzer and J. S. Murray, *ChemPhysChem*, 2020, **21**, 579–588.
35 X. Wang, Z. Niu, Q. Li and S. Scheiner, *Inorg. Chem.*, 2024, **63**, 14656–14664.
36 N. Liu, Q. Li, S. Scheiner and X. Xie, *Phys. Chem. Chem. Phys.*, 2022, **24**, 15015–15024.
37 W. Li, Y. Zeng, X. Li, Z. Sun and L. Meng, *Phys. Chem. Chem. Phys.*, 2016, **18**, 24672–24680.
38 S. Scheiner, *Phys. Chem. Chem. Phys.*, 2024, **26**, 27382–27394.
39 A. Bauza and A. Frontera, *Phys. Chem. Chem. Phys.*, 2015, **17**, 24748–24753.
40 M. Michalczyk, W. Zierkiewicz and S. Scheiner, *Phys. Chem. Chem. Phys.*, 2024, **26**, 5836–5847.
41 A. Bauzá, A. Frontera and T. J. Mooibroek, *Chem. – Eur. J.*, 2019, **25**, 13436–13443.
42 M. Solimannejad, V. Ramezani, C. Trujillo, I. Alkorta, G. Sánchez-Sanz and J. Elguero, *J. Phys. Chem. A*, 2012, **116**, 5199–5206.
43 L. Zhang and D. Li, *Int. J. Quantum Chem.*, 2021, **121**, e26531.

44 W. Zierkiewicz, M. Michalczyk and S. Scheiner, *Phys. Chem. Chem. Phys.*, 2018, **20**, 4676–4687.
45 C. Gatti, A. Dessì, R. Dallocchio, V. Mamane, S. Cossu, R. Weiss, P. Pale, E. Aubert and P. Peluso, *Molecules*, 2020, **25**, 4409.
46 H. Wang, C. Li, W. Wang and W. J. Jin, *Phys. Chem. Chem. Phys.*, 2015, **17**, 20636–20646.
47 S. Scheiner, *J. Chem. Phys.*, 2021, **155**, 174302.
48 A. Ruigrok van der Werve, Y. R. van Dijk and T. J. Mooibroek, *Chem. Commun.*, 2018, **54**, 10742–10745.
49 V. d. P. N. Nziko and S. Scheiner, *Phys. Chem. Chem. Phys.*, 2016, **18**, 3581–3590.
50 A. Amonov and S. Scheiner, *J. Phys. Chem. A*, 2024, **128**, 8751–8761.
51 B. Mallada, M. Ondráček, M. Lamanec, A. Gallardo, A. Jiménez-Martín, B. de la Torre, P. Hobza and P. Jelínek, *Nat. Commun.*, 2023, **14**, 4954.
52 A. V. Rozhkov, S. Burguera, A. Frontera and V. Y. Kukushkin, *Cryst. Growth Des.*, 2024, **24**, 9581–9589.
53 A. V. Rozhkov, E. A. Katlenok, M. V. Zhmykhova, A. Y. Ivanov, M. L. Kuznetsov, N. A. Bokach and V. Y. Kukushkin, *J. Am. Chem. Soc.*, 2021, **143**, 15701–15710.
54 P. R. Varadwaj, H. M. Marques, A. Varadwaj and K. Yamashita, *Cryst. Growth Des.*, 2024, **24**, 7789–7807.
55 F. Weigend, *Phys. Chem. Chem. Phys.*, 2006, **8**, 1057–1065.
56 Y. Zhao and D. G. Truhlar, *Acc. Chem. Res.*, 2008, **41**, 157–167.
57 Y. Zhao and D. G. Truhlar, *Theor. Chem. Acc.*, 2008, **120**, 215–241.
58 M. J. Frisch, G. W. Trucks, H. B. Schlegel, G. E. Scuseria, M. A. Robb, J. R. Cheeseman, G. Scalmani, V. Barone, G. A. Petersson, H. Nakatsuji, X. Li, M. Caricato, A. V. Marenich, J. Bloino, B. G. Janesko, R. Gomperts, B. Mennucci, H. P. Hratchian, J. V. Ortiz, A. F. Izmaylov, J. L. Sonnenberg, D. Williams-Young, F. Ding, F. Lipparini, F. Egidi, J. Goings, B. Peng, A. Petrone, T. Henderson, D. Ranasinghe, V. G. Zakrzewski, J. Gao, N. Rega, G. Zheng, W. Liang, M. Hada, M. Ehara, K. Toyota, R. Fukuda, J. Hasegawa, M. Ishida, T. Nakajima, Y. Honda, O. Kitao, H. Nakai, T. Vreven, K. Throssell, J. A. Montgomery Jr., J. E. Peralta, F. Ogliaro, M. J. Bearpark, J. J. Heyd, E. N. Brothers, K. N. Kudin, V. N. Staroverov, T. A. Keith, R. Kobayashi, J. Normand, K. Raghavachari, A. P. Rendell, J. C. Burant, S. S. Iyengar, J. Tomasi, M. Cossi, J. M. Millam, M. Klene, C. Adamo, R. Cammi, J. W. Ochterski, R. L. Martin, K. Morokuma, O. Farkas, J. B. Foresman and D. J. Fox, *Gaussian-16*, Gaussian, Inc., Wallingford, CT, 2016.
59 G. Paytakov, T. Dinadayalane and J. Leszczynski, *J. Phys. Chem. A*, 2015, **119**, 1190–1200.
60 B. S. D. R. Vamhindi and A. Karton, *Chem. Phys.*, 2017, **493**, 12–19.
61 R. Podeszwa and K. Szalewicz, *J. Chem. Phys.*, 2012, **136**, 161102.
62 S. Karthikeyan, V. Ramanathan and B. K. Mishra, *J. Phys. Chem. A*, 2013, **117**, 6687–6694.
63 M. Majumder, B. K. Mishra and N. Sathyamurthy, *Chem. Phys.*, 2013, **557**, 59–65.
64 M. A. Vincent and I. H. Hillier, *Phys. Chem. Chem. Phys.*, 2011, **13**, 4388–4392.
65 A. D. Boese, *ChemPhysChem*, 2015, **16**, 978–985.
66 M. Walker, A. J. A. Harvey, A. Sen and C. E. H. Dessent, *J. Phys. Chem. A*, 2013, **117**, 12590–12600.
67 L. F. Molnar, X. He, B. Wang and K. M. Merz, *J. Chem. Phys.*, 2009, **131**, 065102.
68 S. F. Boys and F. Bernardi, *Mol. Phys.*, 1970, **19**, 553–566.
69 T. Lu and F. Chen, *J. Mol. Graphics Modell.*, 2012, **38**, 314–323.
70 T. Lu and F. Chen, *J. Comput. Chem.*, 2012, **33**, 580–592.
71 T. A. Keith, *TK Gristmill Software*, Overland Park KS, 2013.
72 R. F. W. Bader, *J. Phys. Chem. A*, 1998, **102**, 7314–7323.
73 P. L. A. Popelier, *Atoms in Molecules. An Introduction*, Prentice Hall, Harlow, UK, 2000.
74 A. Bauzá and A. Frontera, *Angew. Chem., Int. Ed.*, 2015, **54**, 7340–7343.
75 E. Makarewicz, J. Lundell, A. J. Gordon and S. Berski, *J. Comput. Chem.*, 2016, **37**, 1876–1886.
76 S. J. Grabowski, *Crystals*, 2022, **12**, 112.
77 W. Zierkiewicz, M. Michalczyk and S. Scheiner, *Molecules*, 2021, **26**, 1740.
78 W. Zierkiewicz, R. Wysokiński, M. Michalczyk and S. Scheiner, *Phys. Chem. Chem. Phys.*, 2019, **21**, 20829–20839.

